On intermediate-scale open-sea experiments on floating offshore structures: Feasibility and application on a spar support for offshore wind turbines

On intermediate-scale open-sea experiments on floating offshore structures: feasibility and application on a spar support for offshore wind turbines

Carlo Ruzzo[1], Vincenzo Fiamma[1], Maurizio Collu[2], Giuseppe Failla[1], Vincenzo Nava[3], Felice Arena[1]

[1] Natural Ocean Engineering Laboratory (NOEL), Mediterranea University, Reggio Calabria, Italy.

[2] Cranfield University, Cranfield, United Kingdom.

[3] Tecnalia Research and Innovation, Energy and Environment Division, Derio, Spain & Basque Centre for Applied Mathematics BCAM, Bilbao, Spain.

Abstract

Experimental investigation of floating structures represents the most direct way for achieving their dynamic identification and it is particularly valuable for relatively new concepts, such as floating supports for offshore wind turbines, in order to fully understand their dynamic behaviour. Traditional experimental campaigns on floating structures are carried out at small scale, in indoor laboratories, equipped with wave and wind generation facilities. This article presents the results of a 1:30 open-sea experimental activity on a scale model of the OC3-Hywind spar, in parked rotor conditions, carried out at the Natural Ocean Engineering Laboratory (NOEL) of Reggio Calabria (Italy). The aim of the experiment is two-fold. Firstly, it aims to assess the feasibility of low-cost, intermediate-scale, open-sea activities on offshore structures, which are proposed to substitute or complement the traditional indoor activities in ocean basins. Secondly, it provides useful experimental data on damping properties of spar support structures for offshore wind turbines, with respect to heave, roll and pitch degrees of freedom. It has been proven that the proposed approach may overcome some limitations of traditional small-scale activities, namely high costs and small scale, and allows to enhance the fidelity of the experimental data currently available in literature for spar floating supports for offshore wind turbines.

Keywords

1. Offshore structures
2. Spar
3. Floating wind turbines
4. Physical model
5. Heave damping
6. Roll damping

Introduction

Nowadays, floating structures are used by several industries, including oil & gas, renewables (wind, wave, tidal), ports, and others, while the development and spread of many further concepts is envisaged to take place in a near future [1]. In the case of offshore wind industry, several advantages in moving offshore wind energy production towards deep waters can be exploited, including the availability of larger areas, stronger and steadier winds, and the reduction of visual and acoustic impact. However, the development of such concepts requires a significant amount of research in multiple areas of knowledge, including the

development of reliable dynamic models, able to represent the coupled behaviour of the floating wind turbines [2-3]. While such models are usually implemented by means of numerical codes [4-5], experimental activities play a crucial role for their validation, as well as for the system identification.

The experimental activities on floating offshore wind turbines may be classified in two groups, namely small-scale and large-scale ones. Traditional small-scale activities (1:50-1:100) are carried out in controlled environment such as wave tanks and ocean basins, where the desired wind-wave conditions can be reproduced, to measure the dynamic response of the structure and to calibrate opportunely the numerical codes [6-8]. Although the controlled environment allows to achieve very precise and reliable results, these activities have some relevant disadvantages, namely high rental fees of the basins, limited duration of the experiments, and limitations in representing all the relevant physical phenomena at scale level, which may alter significantly the dynamic behaviour of the model with respect to the full-scale structure. On the opposite side, large-scale activities (1:1-1:10) are carried out in open-sea and allow to represent all the relevant features of the offshore wind turbines, including turbine-support interaction, mooring system and grid connection, in relevant operational conditions [9-11]. Clearly, such projects are very expensive and usually represent pilot activities, which are carried out by big companies and/or public bodies for demonstration and commercial purposes, and whose results are rarely publicly available.

1.1 Literature review

Up to now, several small-scale and large-scale experimental activities have been conducted on spar support structures for offshore wind turbines, aimed to prove the feasibility of the concept and validate the corresponding numerical models. A full-scale prototype of a 2.3 MW spar floating offshore wind turbine was installed in 2009 by Statoil [12], off the coast of Norway, on a water depth of about 200 m. The project, called “Hywind Demo”, has proved the technical feasibility of the spar configuration for floating offshore wind turbines, but neither the detailed design characteristics of the offshore wind turbine, nor the recorded field data are publicly available. In 2006, a 1:47 scale model of a 5-MW spar floating wind turbine was tested by Nielsen et al. [13] at the Ocean Basin Laboratory of Marintek, in Trondheim (Norway). The model was tested in irregular waves and turbulent wind speed and various control strategies were adopted. The experimental data showed relatively good agreement with the numerical results obtained in SIMO/RIFLEX, however some information were not released, concerning the detailed characteristics of the model. In 2010, the Offshore Code Comparison (OC3) project [4] was established to verify the accuracy and correctness of the most commonly used numerical codes for coupled analysis of offshore wind turbines. Within this project, the OC3-Hywind spar buoy [14] was defined as the reference spar concept designed to support the NREL-5MW reference offshore wind turbine [15]. Since then, this concept has been widely used for experimental studies on offshore wind turbines, since Statoil’s Hywind characteristics are not released for public use. In 2011, a 1:128 scale model of the OC3-Hywind platform was tested by Shin [16] at the Ocean Engineering Wave Tank of the University of Ulsan (South Korea). The experiment was conducted under various environmental conditions, including regular waves, associated to constant wind speed and rotating rotor, and irregular waves, associated to fixed rotor. Response Amplitude Operators (RAOs) and significant motions were obtained and compared to numerical predictions obtained using FAST and MOSES codes. In 2010, the Japanese Ministry of Environment started a national demonstration project which led to the installation of a 1:2.35 (2012) and a 1:1 (2013) grid-connected 100 kW and 2 MW spar wind turbines off Goto Islands (Japan), preceded by the testing of a 1:100 scale model, in the offshore structure basin of National Maritime Research Institute (NMRI) in Tokyo (Japan), and of a 1:10 model at sea [9-10,17]. The small-scale test was aimed to study the dynamic behaviour of the model, particularly concerning the effects of blade-pitch control, under regular and irregular waves and constant wind speed. The 1:10 model was

aimed to further assess the safety and the performances of the chosen concept. Limited information are available concerning the 1:1 test activity, while experimental data collected in 2012 during a severe typhoon were compared to numerical predictions in FAST by Utsunomiya et al. [18], revealing quite good agreement. In 2012, a 1:50 scale-model of a spar floating wind turbine was tested within a project conducted by the University of Maine [19-20], aimed to compare it with a semi-submersible and a Tension-Leg Platform model. The three models were tested at Maritime Research Institute Netherlands (MARIN) in Wageningen (Netherlands) under various wind-wave conditions, including dynamic wind and bi-directional sea states. Full system identification was achieved, including estimation of the damping ratios and the RAOs. In 2013, a 1:100 scale model of a stepped-spar was tested by Sethumaran and Venugopal [21] at the curved wave tank of the University of Edinburgh (Scotland, UK). Only hydrodynamic behaviour of the model was investigated through regular and irregular wave tests and the experimental results in the frequency (RAOs) and time domain were compared to numerical predictions obtained using Orcaflex code. Also, different mooring systems were tested and their performances were compared. In 2016, a 1:50 scale model of OC3-Hywind spar was tested at MARIN by Duan et al. [22], who obtained response spectra for various load combinations and provided a deeper insight on the coupled dynamics of spar floating wind turbines. All these activities provided useful experimental results on the spar dynamic behaviour, but suffered from the above-mentioned limitations, in particular concerning the relatively high costs associated to basin rental, the restrictions in experimental duration and the insurgence of scale effects.

1.2 Aim

The purpose of this paper is to present the results of a 1:30 scale experimental activity on a spar floating support for offshore wind turbines, carried out near shore at the Natural Ocean Engineering Laboratory (NOEL) of Reggio Calabria (Italy). The support model tested is inspired to OC3-Hywind and has been represented in parked rotor conditions. The experimental activities carried out during this campaign were aimed at addressing and solving some of the problems inherent to the traditional experimental activities in ocean basins (some initial results were published in references [23-24]).
In recognition of the fact that the well-known identification techniques adopted in indoor laboratories must be modified to work in a non-controlled marine environment, this paper offers a broad-wide overview about the requirements, test methodologies, instrumentations and identification methods necessary for operating dynamic identification of offshore floating structures' intermediate-scale models in open-sea conditions. Then, the results obtained from the free decay tests and the irregular wave tests performed on the 1:30 spar structure are presented in terms of RAOs, damping coefficients and significant motions in heave, roll and pitch, in order to calibrate a numerical model of the structure implemented through the software Ansys AQWA [25-26]. These experimental data represent valuable and original information on the hydrodynamic behaviour of the OC3-Hywind platform, since the scale factor chosen for the model is sufficiently high to minimize the scale effects in the representation of wave forces. Finally, the feasibility of the new approach proposed is discussed and its main advantages and limitations are outlined.

Experimental set-up

2.1 Suitable test site characteristics

The choice of the test site is a crucial step for the arrangement of intermediate-scale, open-sea, experimental activities, since local wind-wave conditions must fulfil some restrictive requirements. First of all, the local waves at the test site must be representative of the full-scale conditions, according to Froude scaling laws. As observed by Boccotti [27], such a condition can be obtained if the wave spectrum of the

model waves is a scale model of the design spectrum at all the water depths. Such a requirement is particularly important when dealing with deep-drafted structures, such as spar buoys, and is challenging to achieve in open sea, since smaller sea states are usually made up of wind-generated waves superimposed by swells, which have a higher impact on the water particle kinematics at deeper levels and alter significantly the similitude with respect to full-scale wind-generated design sea states. On the other hand, it is known that, while small wind-generated sea states are essential for modelling the dynamic response in Froude scale, confused and mixed sea-states play a crucial role for the realization of this kind of experimental activities. Indeed, although they do not represent in scale any realistic condition, they allow to investigate the response of the model structure over a larger frequency range, possibly close to its natural frequencies, so that estimation of RAOs and damping coefficients can be achieved. Finally, the test site should present other characteristics, favourable for field experiment activities [27].

The test site chosen for the present study is the Natural Ocean Engineering Laboratory (NOEL), located in the sea front of Reggio Calabria (Italy), on the eastern coast of Messina's Strait (LAT 38°06.538'N; LONG 15°38.478'E) (Fig.1). The site is particularly favourable for the selected case study, since it presents small wind-generated sea states with significant wave heights H_s between 0.20 m and 0.40 m, peak periods T_p between 1.8 s and 2.6 s and JONSWAP-like spectra, which occur regularly, as well as the required variety of wave loading condition for model identification over a relatively large frequency range. The realization of these sea states is due to the unique environmental and geographical characteristics of the area, i.e. the local NNW wind, blowing from Sicily with a high stability, the orientation of the coast from SW to NE, sheltering the swells coming from South and the relatively small fetch, which is about 10^4 m. Finally, the tide amplitude is within 0.1 m: such a small value is of crucial importance for experimental testing of offshore structures, since larger variations of the water depth may affect significantly the operation of the mooring system. A detailed description of the test site metocean conditions is available in ref. [27-29]

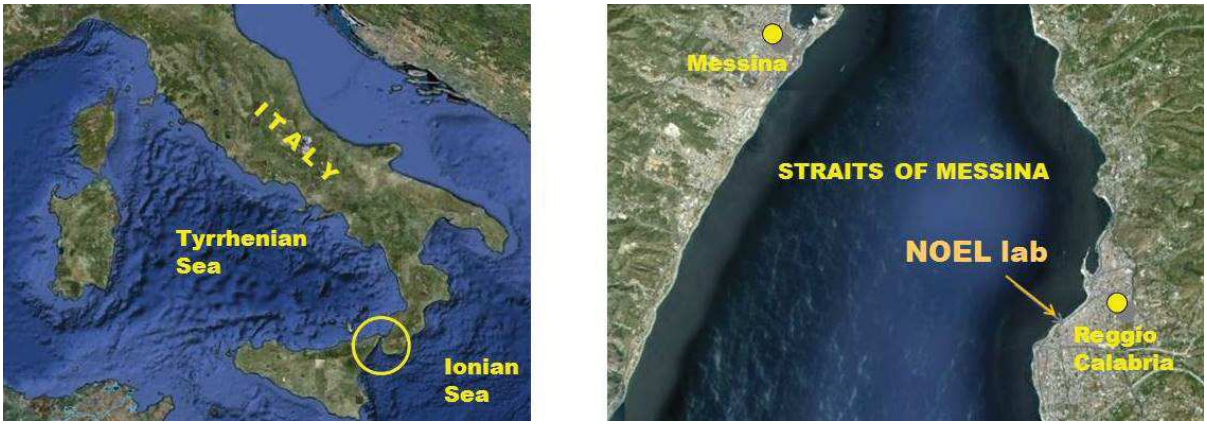

Figure 1 – NOEL site [29].

2.2 Importance of scale effects for spar structures

The Froude scaling laws, in terms of the variables of interest for the scale models of floating wind turbines, are reported in Table 1.

Table 1 – Froude scaling laws for physical models of offshore wind turbines

Parameter	*Scale factor*	*Units*
Length	λ_L	m
Angle	$\lambda_\theta = 1$	rad
Time	$\lambda_T = \lambda_L^{0.5}$	s
Velocity	$\lambda_v = \lambda_L^{0.5}$	m s^{-1}
Angular velocity	$\lambda_\omega = \lambda_L^{-0.5}$	rad s^{-1}
Acceleration	$\lambda_a = 1$	m s^{-2}
Density	$\lambda_\rho = 1$	kg m^{-3}
Mass	$\lambda_m = \lambda_L^3$	kg
Mass moment of inertia	$\lambda_I = \lambda_L^5$	kg m^2
Force	$\lambda_F = \lambda_L^3$	N
Power	$\lambda_P = \lambda_L^{3.5}$	W
Keulegan-Carpenter number	$\lambda_K = 1$	-
Reynolds number	$\lambda_R = \lambda_L^{1.5}$	-

In Table 1, Keulegan-Carpenter number K_C and Reynolds number R_e are defined as functions of the maximum wave velocity v_{max}, a characteristic wave period T, which is usually identified as the peak period of the sea state, a characteristic length of the structure D, which is usually identified as its diameter, and the water kinematic viscosity ν:

$$K_C = \frac{v_{\max} T}{D} \tag{1}$$

$$R_e = \frac{v_{\max} D}{\nu} \tag{2}$$

As Froude scale inevitably alters Reynolds number R_e, several challenges arise in the scale representation of the wind turbine and support hull. Since in this work only the parked rotor conditions will be investigated, a detailed treatment of the scaling procedures regarding the wind turbine will not be further discussed, see for example [30-32]. Regarding the hull, wave-structure interaction depends on the relative size of the structure with respect to the wavelength. Morison's equation [33] can be adopted when the spar radius R is smaller than $0.10L$, being L a characteristic wave length, representative of the sea state [34]. According to Jonkman, [14], such a condition is fulfilled for all the most relevant operational and ultimate conditions of the OC3-Hywind spar buoy, hence the unit wave force vector on the hull may be expressed as the following function of the vertical distance z from still water level:

$$\begin{aligned}\mathbf{f}(z,t) = (1+C_a)\rho\pi R^2(z)\mathbf{a}(z,t) - C_a\rho\pi R^2(z)\ddot{\mathbf{u}}(z,t) + \\ + C_d\rho R(z)\left|\mathbf{v}(z,t)-\dot{\mathbf{u}}(z,t)\right|\left[\mathbf{v}(z,t)-\dot{\mathbf{u}}(z,t)\right]\end{aligned} \tag{3}$$

where $\dot{f}$ represents the time derivative of function f, ρ is the water density, **v** and **a** are wave velocity and acceleration vectors, and **u** is the structure rigid body motion vector. The added mass and drag coefficients C_a and C_d generally depend on Keulegan-Carpenter and Reynolds numbers [35] but they can be assumed constant if the following condition is fulfilled [27]:

$$R_e > 10^4 K_C \tag{4}$$

Condition (4) is generally satisfied for full-scale offshore wind turbine spar under all the most relevant wave conditions [23], but the same may not be true for the corresponding small-scale models. Indeed, the Reynolds number scales with a factor equal to $\lambda_L^{1.5}$, hence condition (4) may be violated for smaller models, resulting in scale effects due to the alteration of the hydrodynamic coefficients, which describe wave-structure interaction (see, or example references [36-37]).

Other challenges related with the scaling of floating structures concern the mass distribution of the structure and the mooring system. It is almost impossible, indeed, to scale down exactly all the structural properties, e.g. wall thickness, because manufacturing as well as strength requirements of the scale model must be taken in due consideration. Hence, in general it shall be ensured that the scale model matches the full-scale structure in terms of global properties such as mass, position of the centre of gravity, mass moments of inertia and mooring linearized stiffness. Also in this case, the smaller is the model, the more challenging is to fulfil these requirements.

2.3 Description of the 1:30 spar model

The OC3-Hywind spar buoy is basically a vertical tapered cylinder, moored to seabed by three catenary lines, and supporting the NREL-5MW reference offshore wind turbine [14]. The 1:30 model installed at NOEL (Fig. 2) is made up of a steel hull and an aluminium tower, separated by a plastic disc to avoid galvanic corrosion. The hull has been ballast-stabilized by steel discs deployed in its lower section, so that the required position of the centre of gravity has been achieved. The rotor-nacelle assembly (RNA) has been modelled as a lumped mass at the top of the tower. The main geometry and mass characteristics are reported, respectively, in Table 2 and Table 3, while some additional details on the design of the model are described in Ref. [23].

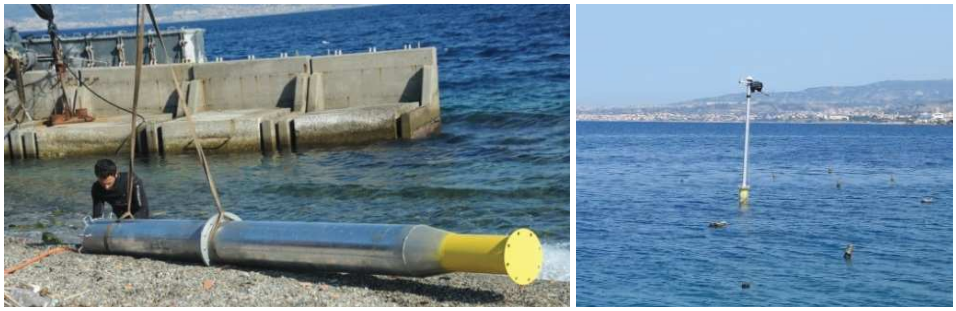

Figure 2 – Spar hull model before (left) and after (right) installation, sustaining the parked turbine model [29]

Table 2 – Geometry of the structure at model scale and full scale and comparison with the OC3-Hywind.

Parameter	*Units*	*Scale model (1:30)*	*Full-scale structure (1:1)*	*OC3-Hywind (1:1)*
Diameter	m	0.217; 0.313	6.51; 9.39	6.50; 9.40
Draft	m	3.884	116.5	120.0
Centre of buoyancy, vertical position (from SWL)	m	-1.974	-59.21	-62.06
Taper, vertical position	m	-0.020; -0.287	-0.61; -8.62	-4.00; -12.00

(from SWL)				
RNA, vertical position (from SWL)	m	3.080	92.39	90.00

202

203 *Table 3 – Mass characteristics of the structure at model scale and full scale and comparison with the OC3-*
204 *Hywind.*

Parameter	*Units*	*Scale model (1:30)*	*Full-scale structure (1:1)*	*OC3-Hywind (1:1)*
Total mass	kg	297.0	$8.02 \cdot 10^6$	$8.07 \cdot 10^6$
Centre of gravity, vertical position (from SWL)	m	-2.496	-74.88	-78.00
Moment of inertia about x-axis (respect to the CoG)	kg m^2	994.9	$2.42 \cdot 10^{10}$	$2.30 \cdot 10^{10}$
Moment of inertia about y-axis (respect to the CoG)	kg m^2	995.0	$2.42 \cdot 10^{10}$	$2.30 \cdot 10^{10}$
Moment of inertia about z-axis	kg m^2	4.870	$1.18 \cdot 10^8$	$1.91 \cdot 10^8$

205 Based on condition (4), it is possible to estimate how hydrodynamic coefficients of Morison's equation are
206 altered by the scale factor chosen. To this aim, Fig. 3 shows how the ratio between Reynolds number and
207 Keulegan-Carpenter number varies with the scale factor for the spar support considered, assuming the
208 wave peak period T_p at full scale as the characteristic period T and the diameter of the surface-piercing
209 section of the spar hull as the characteristic length D in equations (1-2).

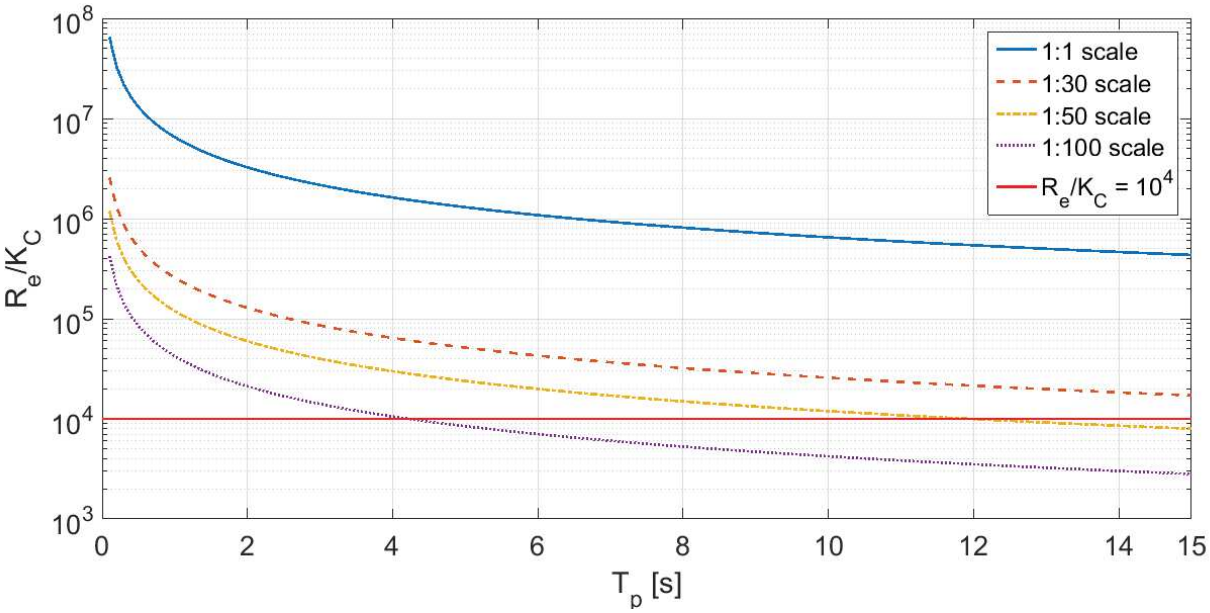

210

211 *Figure 3 – Variation of R_e/K_C ratio depending on the scale factor.*

Fig. 3 confirms that the distortion of Reynolds number at 1:30 scale is rather limited, so that a correct representation of the hydrodynamic coefficients can be achieved in the whole range of peak periods considered. Differently,1:50 models may present slight alterations of the hydrodynamic coefficients for the highest periods (scaled representation of severe storms and swells) and 1:100 models significantly alter Reynolds number, resulting in a distortion of wave forces in the whole range of realistic wave peak periods. This is a significant advantage of intermediate-scale open-sea field experiments in terms of representation of the actual dynamic behaviour of spar floating supports for offshore wind turbines.

The mooring system of the model structure has been designed considering the irregular and inclined seabed at the NOEL site, and the local harshest metocean conditions. It is based on the full-scale mooring system design of UMaine-Hywind spar [38], which is equivalent to OC3-Hywind but intended for a water depth of 200 m instead of 320 m. This reference design, however, has been used only for defining the shape of the mooring system, i.e. three 120°-spaced catenary lines, and the weight per unit length of each line. Differently, the position of the anchors and the length of the lines have been set so as to match local bathymetry and to ensure structure safety under local extreme conditions. Consequently, the resulting mooring system of the model has longer mooring lines and smaller stiffness with respect to the full-scale UMaine Hywind spar structure. Moreover, the model mooring system is asymmetric, due to the different water depths of the sea-side and land-side anchors. The design of each line has been carried out through an in-house quasi-static numerical code, based on the particularization of the catenary equation to inclined seabed conditions. Let us consider a 2-D reference system *Ax'z'* in the plane of the catenary line, originating in the anchor point *A* and pointing towards the structure (*z'* positive upwards). Then, the catenary equation may be written as:

$$z'(x') = \frac{F_{x'}}{w}\cosh\left[\frac{w}{F_{x'}}x' + \operatorname{arcsinh}(\tan\beta_A)\right] - \frac{F_{x'}}{w}\sqrt{1+\tan^2\beta_A} \tag{5}$$

being $F_{x'}$ the horizontal tension of the line, w the weight per unit length and β_A the inclination at the anchor point. At the same time, in the local curvilineal system of the line *Asn* (*s* positive towards the structure), the shape of the line may be expressed as:

$$s(x') = \frac{F_{x'}}{w}\sinh\left[\frac{w}{F_{x'}}x' + \operatorname{arcsinh}(\tan\beta_A)\right] - \frac{F_{x'}}{w}\tan\beta_A \tag{6}$$

The quasi-static shape and restoring force of each line has been obtained as a function of surge and sway structure motions by combining equations (5-6) and the boundary conditions, i.e. the fixed position of the anchor, the variable position of the structure and the length of the line. The resulting restoring forces of the three lines for each structure configuration have been summed in the global 3-D reference system *Gxyz*, to obtain the global restoring forces for the structure. The final design of the lines has been obtained through a trial-and-error procedure to achieve the desired stiffness. The resulting characteristics of the mooring system are reported in Table 4, while Fig. 4-5 show the restoring forces as functions of the surge and sway motions of the model. Although these forces are nonlinear, linearized surge and sway stiffness can be defined as the tangent stiffness of the force-motion function in the equilibrium position. The corresponding linearized behaviour is reported in Fig. 4-5 too. In the installation phase, the yaw stiffness has been enhanced through a delta connection of the mooring lines. The length of each side of the delta has been set equal to about 10% of the corresponding line length, following the practical instructions of Quallen et al.

250 [39]. Additional details on the numerical model used for the design of the mooring system of the model
251 may be found in Ref. [23]. A picture of the mooring system taken after installation is shown in Fig. 6.

252 *Table 4 – Characteristics of the mooring system of the model structure.*

Parameter	*Units*	*Model (1:30)*	
		Sea-side	*Land-side*
Fairleads, vertical position (from SWL)	m	-2.224	-2.224
Anchor depth	m	10.40	2.75
Seabed inclination	°	14.21	18.09
Linear mass of the line	kg m^{-1}	0.159	
Radius anchor-spar centreline	m	14.04	12.92
Line length	m	16.56	13.30
Delta connection length	m	1.50	
Top tension	N	24.06	16.99
Touchdown length	m	4.91	3.15
Linearized surge stiffness	N m^{-1}	37.89	
Linearized sway stiffness	N m^{-1}	42.80	

253

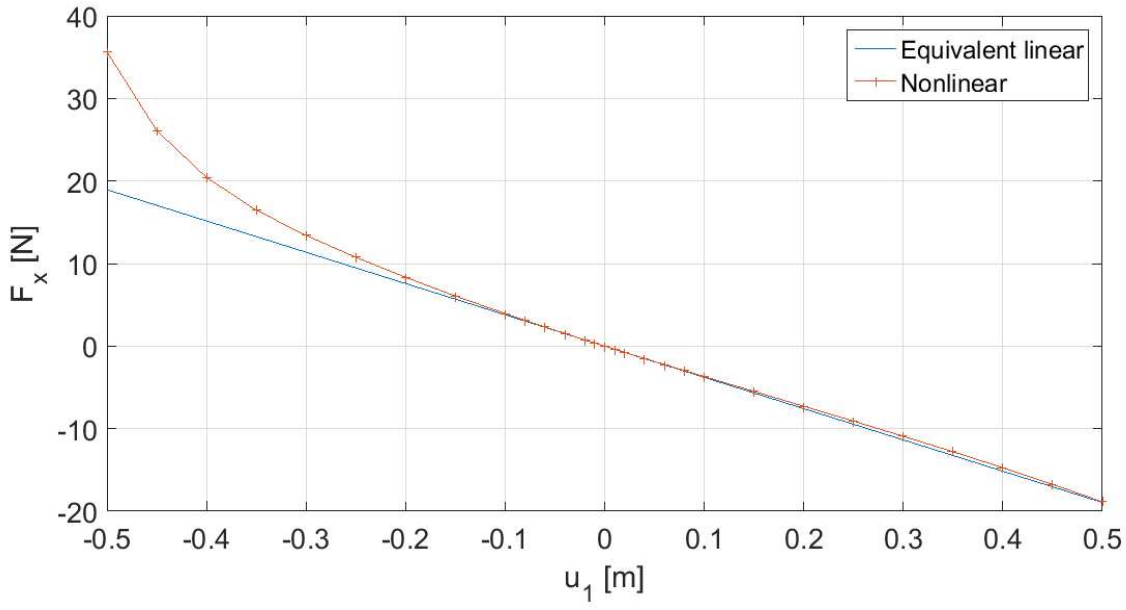

254

255 *Figure 4 –Nonlinear and linearized force-motion behavior of the mooring system of the model in quasi-static*
256 *conditions for surge degree of freedom*

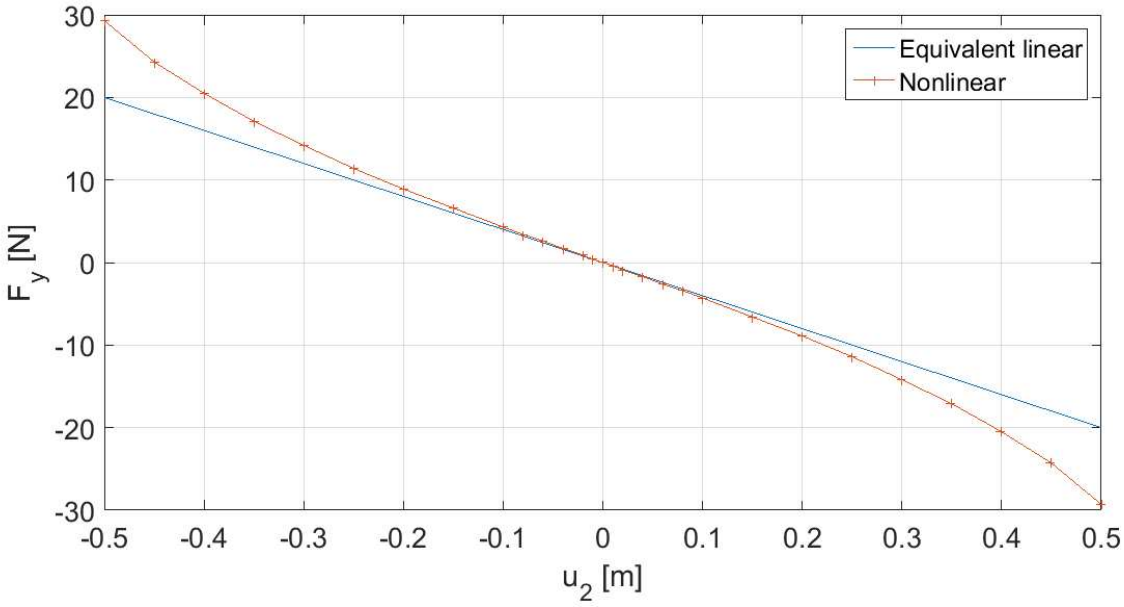

Figure 5 –Nonlinear and linearized force-motion behavior of the mooring system of the model in quasi-static conditions for sway degree of freedom

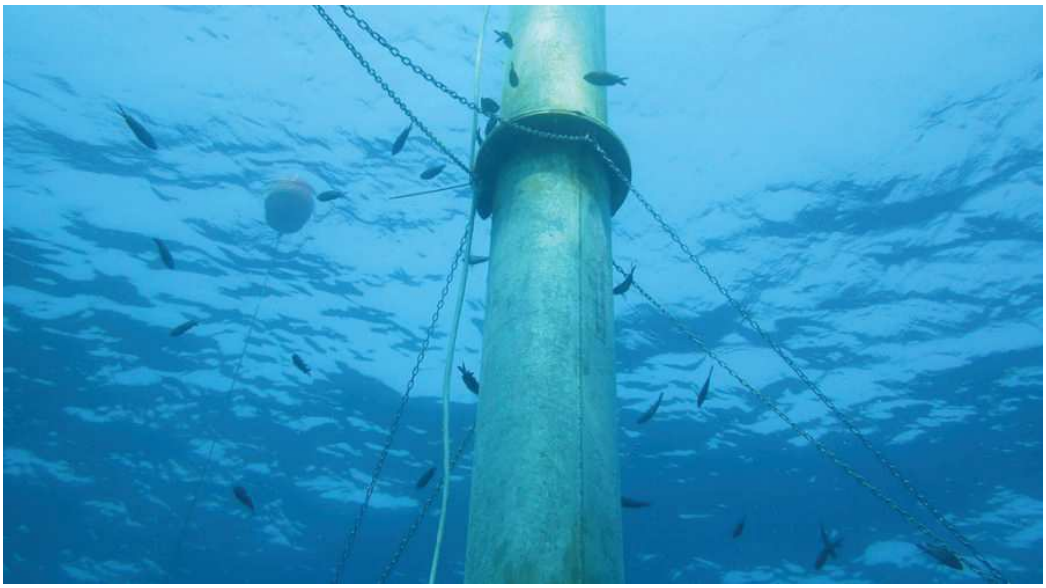

Figure 6 – Catenary mooring system of the model, including delta connections [29]

2.4 Measurement systems

The experimental activity has been carried out using two independent measurement systems.

The first measurement system is for wave data collection, and is made up of two fixed poles, installed close to the spar model, in an undisturbed wave field. Each pole sustains an emerged ultrasonic probe, to measure the time history of the wave surface elevation at a fixed point, and a submerged pressure transducer, to measure the wave pressure time history at the same point, at an average depth of 0.78 m. The four sensors have been synchronized and the correlation factor between ultrasonic probes and

pressure transducers output has been estimated for each sea state, resulting generally greater than 0.85. However, the ultrasonic probes experienced some temporary breakdown (about 28% of data), hence the pressure transducers have been used for the estimations of the wave spectra, due to their greater reliability. Significant wave height, wave spectrum and mean propagation direction for each sea state have been obtained following the methods described in Ref. [27]. Also, the tide variation of the sea level has been calculated for each sea state.

The second system is devoted to the measure of the spar dynamic response, and is composed of a differential global positioning system (DGPS), which returns the position of the structure with respect to a fixed point on the land, and an Attitude and Heading Reference System (AHRS) inertial platform, which measures the inclination of the platform with respect to the three axes.

The two measurements systems have been synchronized, and both have a sampling frequency of 10 Hz.

2.5 Numerical model of the structure

A numerical model of the spar structure has been implemented in ANSYS AQWA (v. 16.1) [26], and has been calibrated with experimental data collected at NOEL. The whole numerical model has been implemented at 1:1 scale, which returns an immediate comparison with OC3-Hywind full-scale structure.

Following the approach of Jonkman [14], the hydrodynamic loads have been modelled adopting a potential theory approach, augmented by the drag term of Morison's equation. According to Jonkman, delta connections of the mooring lines have been represented through an additional yaw stiffness equal to K_{66} = $9.834 \cdot 10^7$ Nmrad^{-1}, and the linear additional damping coefficients B_{11} = B_{22} = $1.000 \cdot 10^5$ Nsm^{-1}, B_{33} = $1.300 \cdot 10^5$ Nsm^{-1}, B_{66} = $1.300 \cdot 10^7$ Nsmrad^{-1} have been added. Initially, the additional damping matrix has been set by Jonkman based on small-scale free decay tests operated by Statoil on a model of the Hywind platform. Then, the additional damping matrix has been calibrated in Section 3.2, using the experimental data collected on the 1:30 model installed at NOEL. The hull has been represented through a "Point mass" item (Table 3), and the mesh includes 6735 diffracting elements (Fig. 7) and 104 line bodies, which are used to include the viscous drag forces. The mooring system has been represented by three catenary lines on a constant water depth of 200 m, sized so that linearized horizontal stiffness is equivalent to the value reported in Table 4 for the structure installed at NOEL.

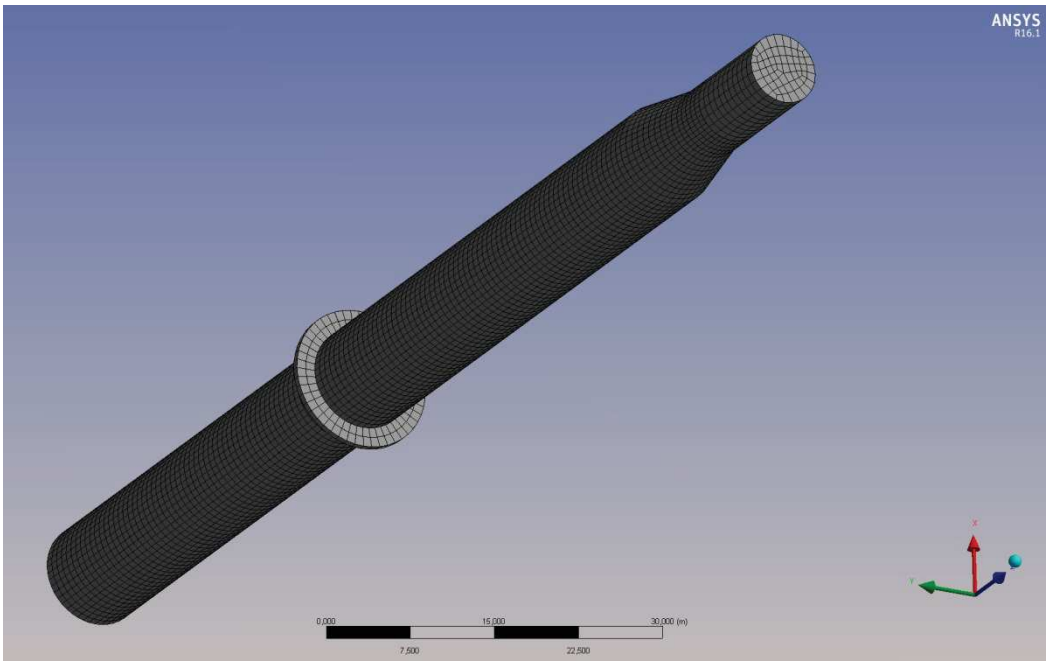

297

298 *Figure 7 – Numerical model of the spar structure in ANSYS AQWA*

299 **3. Results of the experimental activity**

300 The experimental activity on the 1:30 model of OC3-Hywind platform started in July 2015 and was
301 concluded in March 2016. An overall number of 1281 5-minute-long wave and motion records was
302 collected selecting the widest range of local wave conditions possible. The scatter diagrams of significant
303 wave heights with respect to peak periods are shown in Fig. 8.

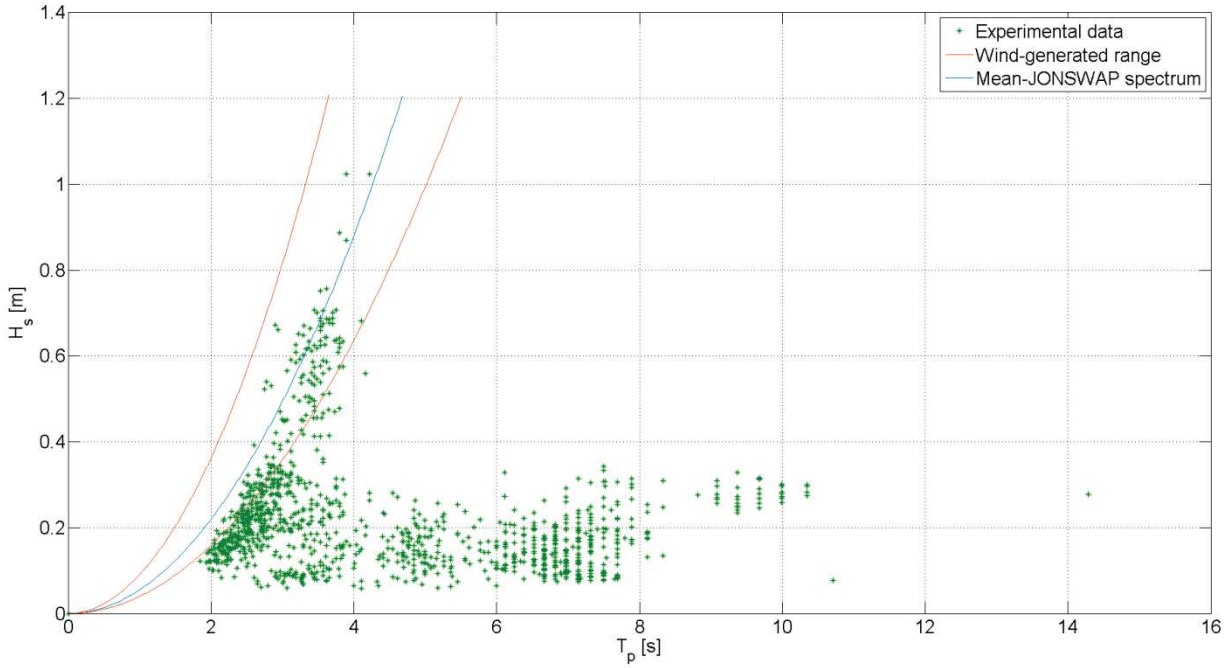

304

305 *Figure 8 – Scatter diagram of the significant wave heights recorded at NOEL with respect to peak period.*

Wave data collected include both wind-generated local sea states, swells and mixed sea states. The wind-generated sea states are useful for the representation of the scaled behaviour of OC3-Hywind in severe wave conditions, while the other ones are important for the determination of the spar characteristics in the frequency domain. The discrimination criterion adopted in Fig. 8 to distinguish wind-generated data is the following:

$$\begin{cases} \psi^* > 0.65 \\ gK_{\min}T_p^{\,2} < H_s < gK_{\max}T_p^{\,2} \end{cases} \tag{7}$$

being ψ^* the narrow-bandedness parameter of the wave head of pressure spectrum defined as in Ref. [27], g the acceleration due to gravity and K_{min}, K_{max} two steepness parameter. The narrow-bandedness parameter is obtained as the module of the minimum of the auto-covariance function of the wave pressure time series, normalized to the maximum of the same function, and tends to unity as the spectrum tends to be infinitely narrow. The first condition in (7) is hence aimed to exclude the mixed sea states, which are relatively broad-banded. The second condition is instead aimed to exclude pure swells, whose steepness is significantly lower than that of wind waves. The limit values of the steepness parameters used in (7) have been derived by Arena et al. [40], considering the whole range of shape parameters of the JONSWAP spectrum, which is representative of wind-generated waves [41]. The resulting limit values are K_{min} = $4.057 \cdot 10^{-3}$ and K_{max} = $9.246 \cdot 10^{-3}$. Overall, 139 wind-generated sea states have been selected from the whole set of 1281 data, using the dual criterion in (7).

3.1 Damping estimations from free decay tests

An estimation of the natural frequencies and damping coefficients of the 1:30 model in heave, roll and pitch has been firstly obtained through free decay tests performed at sea, in sufficiently calm wave conditions ($H_s \leq 0.11$ m) . The procedure for the realization of the tests has been described in Ref. [24]. With respect to the traditional free decay tests carried out in ocean basins, the continuous irregular wave action alters the smallest decay cycles, making the tests shorter and slightly coarser.

The method adopted in this paper for the estimation of damping coefficients is derived from Ref. [42], where extensive description of the method and alternative formulations may be found. In synthesis, for each free decay test, each degree of freedom is treated as uncoupled and thus the corresponding 1-DOF equation of motion is:

$$\left(M_{ii} + A_{ii}\right)\ddot{u}_i + B_{ii}\dot{u}_i + D_{ii}\left|\dot{u}_i\right|\dot{u}_i + C_{ii}u_i = 0 \tag{8}$$

u_i being the degree of freedom (DOF) involved in the free decay test, M_{ii} the corresponding term in the inertia matrix, A_{ii} the hydrodynamic added mass, C_{ii} the stiffness term, B_{ii} the linear damping coefficient and D_{ii} the non-linear damping coefficient. Equation (8) implicitly assumes that the DOFs are not coupled, which is realistic for heave, pitch and roll. By equating the work done by the restoring moment and the energy dissipated by linear and nonlinear damping for each half-cycle (positive or negative) one obtains:

$$\Delta u_{i,peak} = p_1 u_{i,mean} + p_2 u_{i,mean}^2 \tag{9}$$

$$p_1 \equiv \frac{\pi}{2\omega_{n,ii}} \frac{B_{ii}}{\left(M_{ii} + A_{ii}\right)} \tag{10}$$

341 $$p_2 \equiv \frac{4}{3}\frac{D_{ii}}{\left(M_{ii}+A_{ii}\right)} \tag{11}$$

342 $\omega_{n,ii}$ being the natural frequency, which can be read from the test, $u_{i,mean}$ the mean displacement value
343 between two successive peaks (positive or negative) of the test and $\Delta u_{i,peak}$ their difference.

344 In total, 17 free decay tests have been conducted in heave, and 10 in roll/pitch (Fig. 9). Equation (9) has
345 been fitted to the experimental data collected from all the free decay tests, obtaining the curves shown in
346 Fig. 10 and Fig. 11, respectively. The resulting estimations in terms of natural frequencies and linear
347 damping coefficients are reported in Table 5. Interestingly, the estimates of the linear damping coefficients
348 are larger than those suggested by Jonkman [14], which were based on the results of free-decay tests
349 performed on a small-scale model of Statoil's Hywind. This may be due to the relatively large scale of the
350 model, which allows to reduce the scale effects and to obtain a more reasonable approximation of the
351 actual values to be used for the modelling of the full-scale structure.

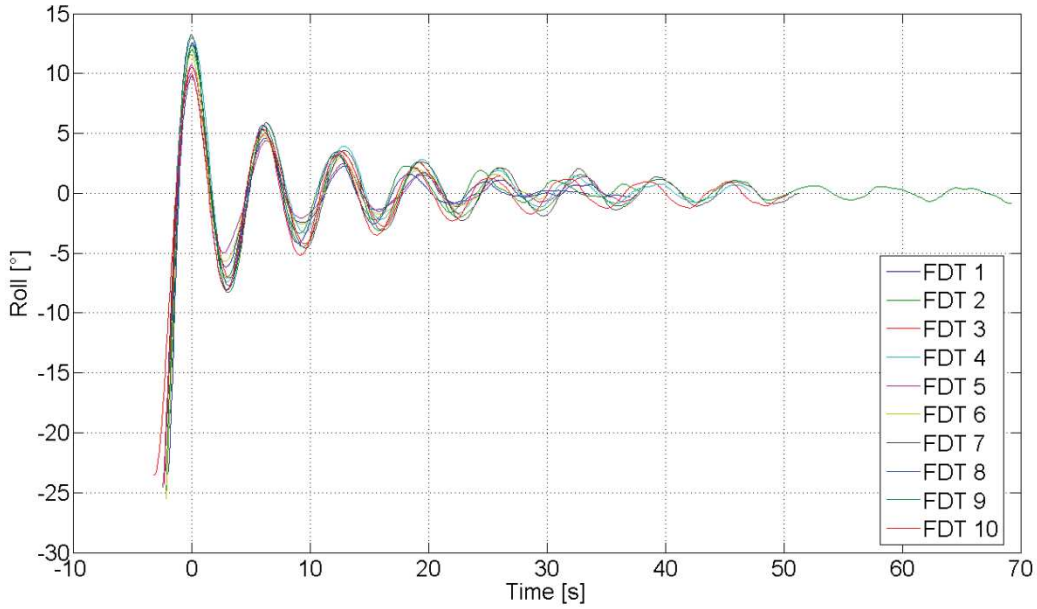

352

353 *Figure 9 – Time histories of the ten roll free decay tests conducted at NOEL.*

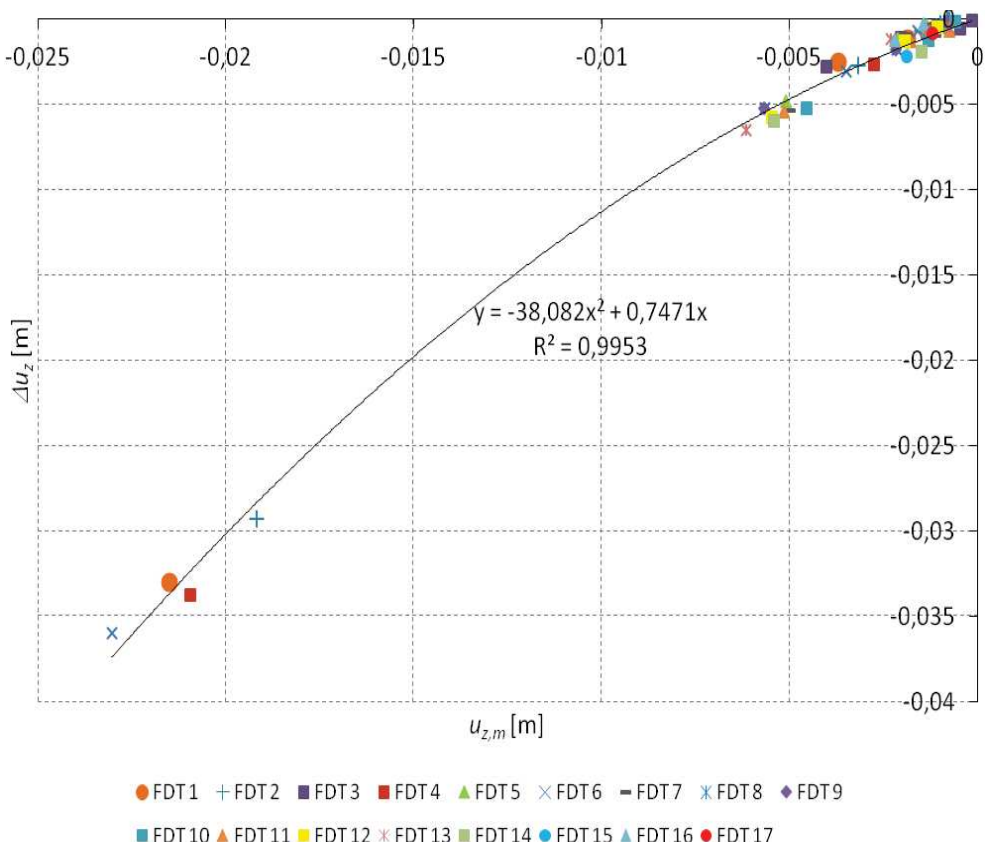

354

355 *Figure 10 – Fitting of Equation (9) to experimental data for the heave degree of freedom.*

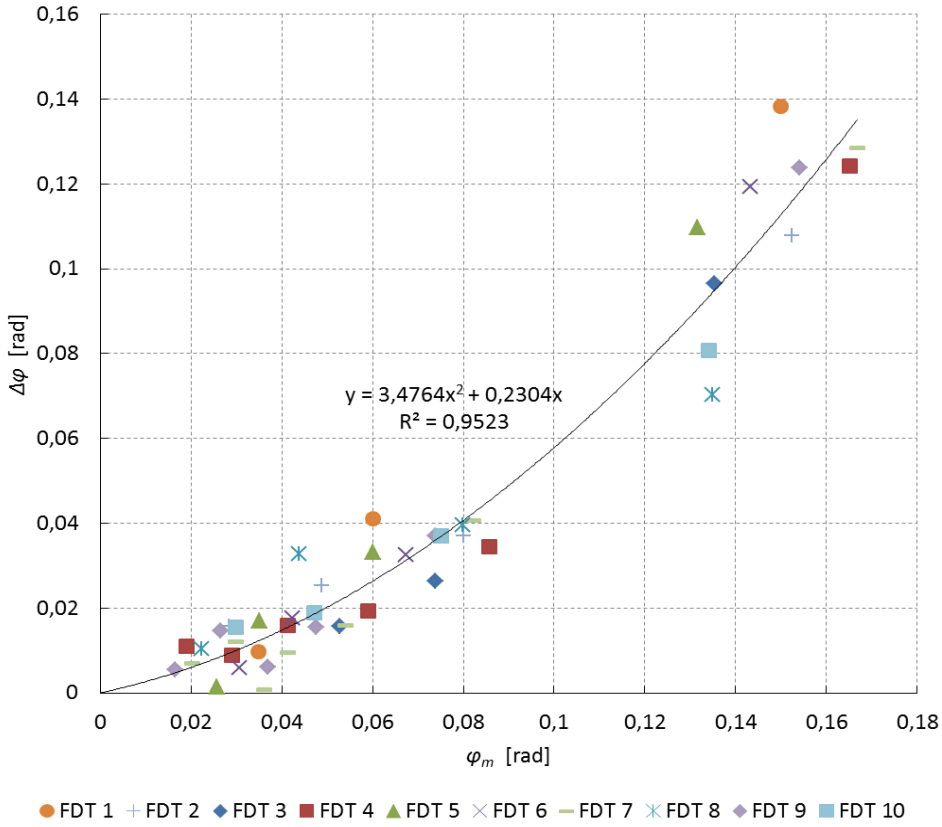

356

Figure 11 – Fitting of Equation (9) to experimental data for the roll degree of freedom.

Table 5 – Experimental estimation of natural frequencies and linear damping coefficients via free decay tests.

Degree of freedom	ω_n *[rad/s]*		B_n *[kg s^{-1}; kg m^2 s^{-1} rad^{-1}]*	
	Model scale (1:30)	*Full-scale (1:1)*	*Model scale (1:30)*	*Full-scale (1:1)*
Heave	1.090	0.199	153.6	$7.570 \cdot 10^5$
Roll/Pitch	1.006	0.202	228.5	$1.014 \cdot 10^9$

The nonlinear damping coefficient D_{roll} has been used instead for the indirect estimation of the hydrodynamic drag coefficient C_d of the hull. It is obtained by equating the nonlinear term of equation (8) and the drag term of the roll moment about the centre of gravity, given by Morison's equation (3). Wave elevation and spar motions in surge and heave have been neglected, so to obtain:

$$C_d = \frac{D_{roll}}{\rho \int_{z_{\min}}^{0} R(z) |z - z_G| (z - z_G)^2 \, dz} \tag{12}$$

z_{min} and z_G being the draft and the centre of gravity position of the model structure, respectively. The resulting value is C_d = 1.998, which is consistent with the expected one for calm water conditions [37]. This represents a further confirmation of the feasibility of Morison's equation for the representation of viscous drag hydrodynamic forces on the spar structure.

3.2 Irregular wave tests: RAOs and damping estimations

A further stage of the model identification has been achieved through the analysis of the spar response to the irregular waves recorded at the test site. The RAOs of the model have been estimated from the experimental data and the numerical model in Ansys AQWA has been calibrated, by setting the linear damping coefficients such that the numerical RAOs fit well the experimental ones. Concerning the nonlinear damping, it has been represented through the drag term of Morison's equation, using a constant drag coefficient C_d = 0.6, representative of the spar behaviour in moderate to severe irregular waves [14], as those measured during the experiment (Fig. 8).

The determination of experimental RAOs in open sea cannot be achieved as in ocean basins, where regular waves and irregular sea states, with the desired broad-banded spectra, can be generated. Consequently, an alternative method for the estimation of the RAOs has been developed and applied to the data collected during the experimental activity, as described below. The relationship between a wave spectrum and the corresponding structure response spectrum, in a given DOF *u*, is expressed by:

$$E_u(\omega) = RAO_u^{\,2}(\omega) E_\eta(\omega) \tag{13}$$

The inverse relationship of equation (13) would give a well-defined estimation of the RAO in the whole frequency domain only when using white noise spectra as input. However, in practice, each sea state has a limited energy content in the frequency domain, i.e. is narrow-banded. For this reason, only the portion of the frequency domain with enough energy content (see Appendix) has been considered for the estimation of experimental RAOs, depending on the wave spectrum of the sea state considered. Following these considerations, each sea state provides information about the RAOs on a limited range of frequencies and a global estimation of the RAOs over the whole frequency domain may be obtained only by averaging over and putting together a sufficient number of data, each contributing to its own frequency range. The expression used in this paper for the estimation of each of these contributions is:

$$RAO_u(\omega) = \sqrt{\frac{E_u(\omega)}{E_{\eta,ph}(\omega)}} \frac{\cosh[k(d+z_{PT})]}{\cosh(kd)} \Leftrightarrow E_{\eta,ph}(\omega) \geq \alpha E_{\eta,ph}(\omega_p) \tag{14}$$

being E_u the motion response spectrum in the u^{th} degree of freedom, $k(\omega)$ the wave number, d the water depth, z_{PT} the distance of the pressure transducer from the still water level, ω_p the peak frequency of the wave spectrum, and α a positive parameter smaller than unity. In the present study, the value chosen for such parameter is α = 0.10 and the portion of the frequency domain considered for the estimation of the RAOs is ω = (0.80 – 4.10) rad/s at model scale (1:30), which corresponds to about ω = (0.15 – 0.75) rad/s at full scale (1:1). Both these values have been calibrated through a parametric analysis, which is described in the Appendix. It should be noted that wave head of pressure spectra $E_{\eta,ph}$ have been used in equation (14) instead of wave surface elevation ones E_η. This is because it has been observed that pressure transducers guarantee greater reliability with respect to ultrasonic probes. The attenuation factor, which depends on the distance z_{PT} of the pressure transducer from the still water level, has been then used to refer the resulting RAO contributions to the wave surface elevation, as it is common practice in offshore engineering.

Due to the axial symmetry of the spar, for the heave RAO estimation it has been possible to use the whole experimental dataset collected at NOEL, i.e. the 1281 sea states and the corresponding time histories of the model structure response, while a selection based on the mean propagation direction value has been made for the estimation of roll and pitch RAOs. In particular, only the sea states with mean propagation directions between -40° and 0° with respect to the North have been included in the dataset considered, obtaining a total number of 824 sea states. The calibration of the numerical model has been made by setting the linear damping coefficients such that the peaks of the numerical RAOs approximately correspond with those of the experimental ones. The estimates obtained through the free decay tests have been used for starting the trial and error fitting procedure. The numerical RAOs used for the calibration process have been obtained in ANSYS AQWA through a linearization process, performed on a sea state with significant wave height of 6 m, mean-JONSWAP spectrum (averaged as in Ref. [27]) and wave propagation direction of -20° (1:1 scale). The resulting experimental and numerical RAOs in heave, roll and pitch at the model scale (1:30) are shown, respectively, in Fig. 12-14. The estimated peak frequencies and damping coefficients are instead reported in Table 6.

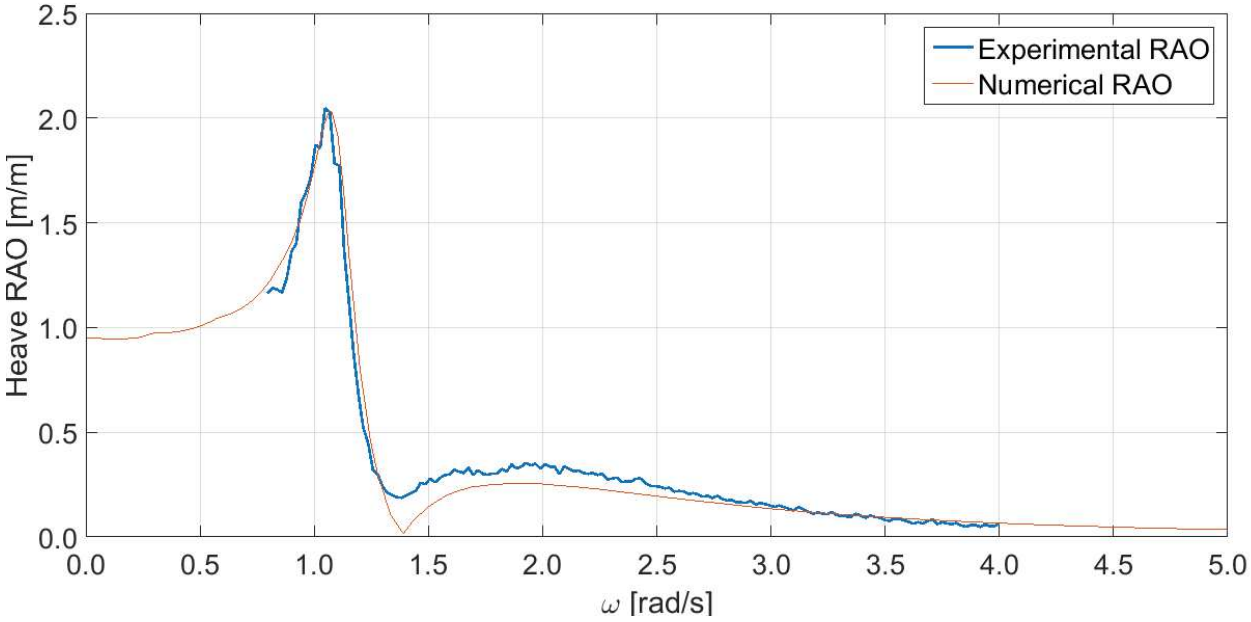

420

421 *Figure 12 – Experimental and numerical heave RAOs at model scale (1:30).*

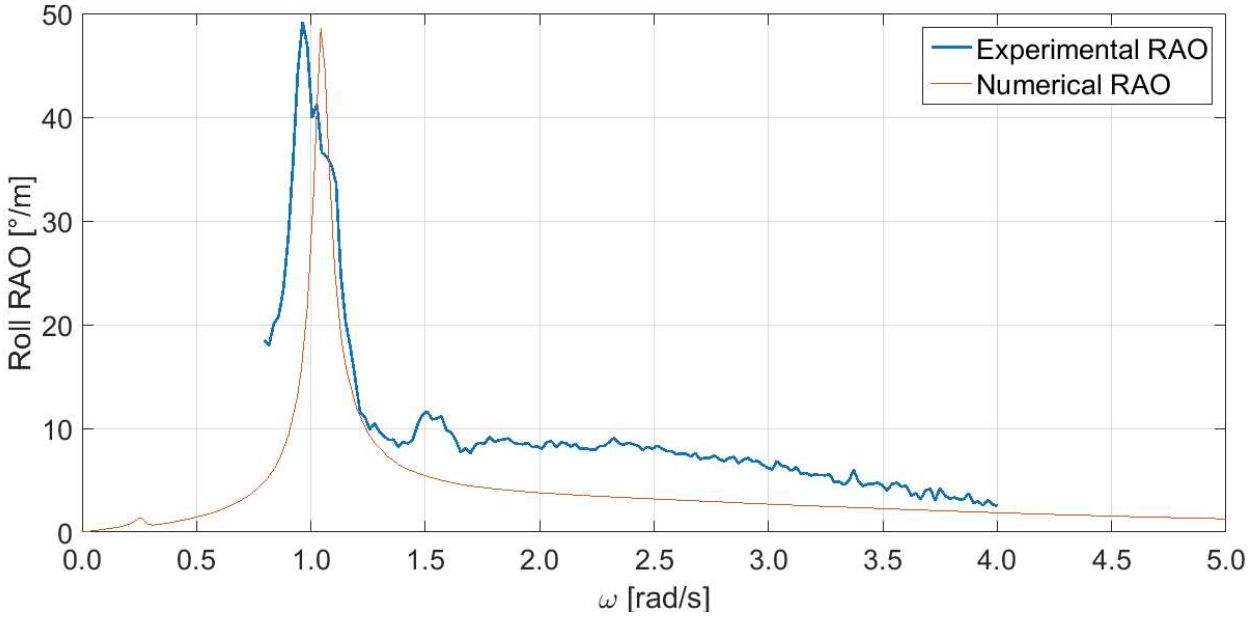

422

423 *Figure 13 – Experimental and numerical roll RAOs at model scale (1:30).*

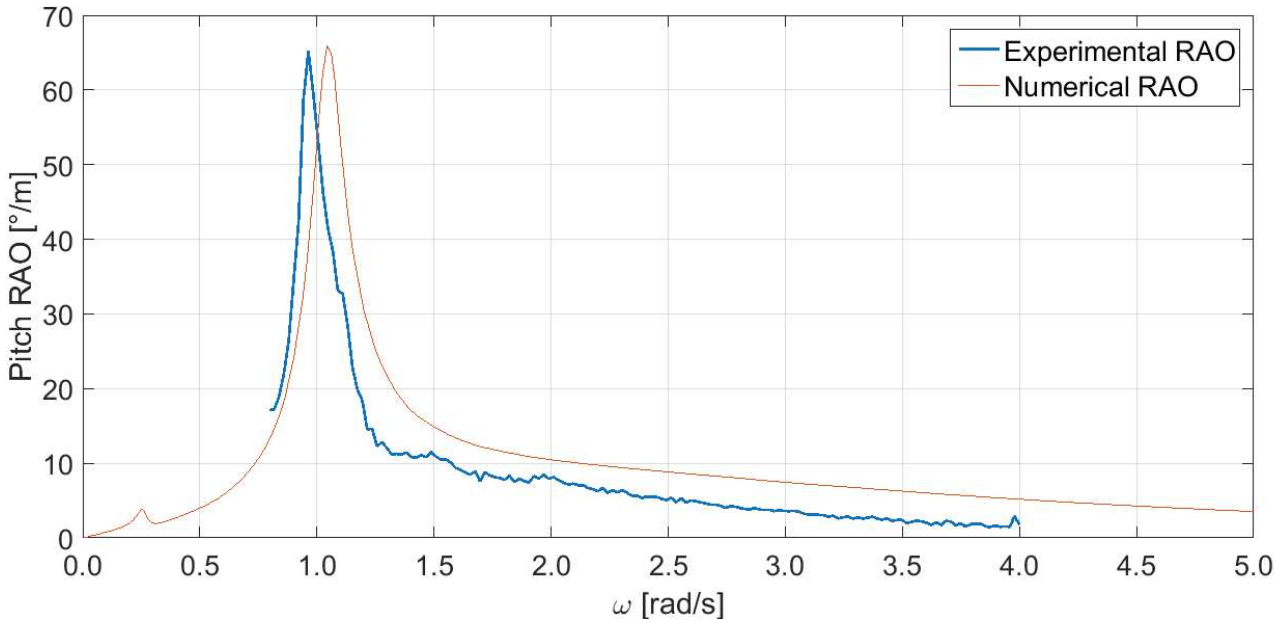

Figure 14 – Experimental and numerical pitch RAOs at model scale (1:30).

Table 6 – Experimental estimation of natural frequencies and linear damping coefficients via irregular wave tests.

Degree of freedom	ω_n *[rad/s]*		B_n *[kg s^{-1}; kg m^2 s^{-1} rad^{-1}]*	
	Model scale (1:30)	*Full-scale (1:1)*	*Model scale (1:30)*	*Full-scale (1:1)*
Heave	1.047	0.191	50.72	$2.500 \cdot 10^5$
Roll	0.963	0.176	89.03	$3.950 \cdot 10^8$
Pitch	0.963	0.176	183.7	$8.150 \cdot 10^8$

Natural frequency estimations obtained via free decay tests (Table 5) and irregular wave tests (Table 6) are consistent to each other, while small differences are observed with respect to the numerical predictions, based on the model characteristics reported in Table 2-3. In particular, the peak frequencies of numerical RAOs are slightly larger than those observed experimentally and the difference is of about 2.5 % for heave and of about 8.1 % for roll and pitch. This is probably due to the inevitable uncertainties introduced in the computation of the mass and mass distribution of the model by multiple causes, including welding and manufacturing procedures, use of non-structural elements such as sensor cables, marine growth and so on. As a result, mass and mass moment of inertia reported in Table 3 are slightly underestimated, resulting in the corresponding overestimation of the natural frequencies.

Linear damping coefficients estimated through irregular waves (Table 6) are instead smaller than those estimated through free decay tests (Table 5), while they are still greater than those predicted by Jonkman [14], based on free decay tests carried out in a small-scale experimental activity. This result leads to interesting conclusions about the feasibility of the free decay tests for the estimation of the model damping coefficients. The estimation of B_n performed by free decay tests is indeed referred to calm water conditions, is based on the hypothesis of uncoupled motions and takes into account the damping properties of the model only around its natural frequencies. Differently, estimation performed through experimental RAOs allow to investigate directly the coupled dynamic behaviour of the model in irregular

445 waves and extends the analysis over a wider frequency range. For these reasons, the latter approach
446 provides more accurate results, which should be used for the calibration of the hydrodynamic numerical
447 models. This encourages the realization of intermediate-scale open-sea experiments on floating supports
448 for offshore wind turbines, since they can provide information concerning the structure dynamic behaviour
449 under relevant wave conditions and at relatively large scales.

450 Another interesting consideration concerns the difference observed in roll-pitch linear damping coefficients
451 estimated through irregular waves (Table 6). Although the model presents some minor asymmetries due to
452 the mooring system and the on-board measurement station, the main cause for that is the directionality of
453 the sea states used for the estimation of the RAOs. Each sea state has indeed different mean propagation
454 directions, which are not uniformly distributed in the range (-40°; 0°), and directional spreading functions.
455 On the opposite side, the sea state used in the numerical model has a single propagation direction (-20°)
456 and no directional spread. In both cases, the dominant rotation of the model is pitch, since the mean
457 propagation direction is close to 0°, however this effect is mitigated in the experiment, where the variability
458 of the mean propagation direction and the directional spread cause an increase of roll motions and a
459 reduction of pitch ones. Consequently, the calibration of the model results in an overestimation of pitch
460 linear damping coefficient, since the directionality of the measured sea states acts as a fictitious additional
461 damping, and in an underestimation of the roll linear damping coefficient, for the opposite reason. The two
462 values obtained for the damping coefficients may be indeed seen as upper and lower bounds, respectively,
463 for pitch/roll linear damping of the spar support. In general, more accurate estimations can be obtained by
464 recording more data, which would allow a finer discretization of the measured wave directional range for
465 the calibration of the numerical model. Differently from roll and pitch, it should be also noted that
466 directionality has no effect in the heave RAO, since heave motion is not affected by wave propagation
467 direction, due to the axial symmetry of the structure.

468 The main drawback of the approach proposed is that no prediction concerning the model structure
469 behaviour could be made outside the envelope of the frequency ranges of the sea states considered (ω =
470 0.80 – 4.10 rad/s), due to the scarcity of sea states with sufficient energy content at the corresponding
471 frequencies. Consequently, the dynamic identification of the model in surge, sway and yaw degrees of
472 freedom could not be realized through the experimental estimation of the RAOs. Nevertheless, some useful
473 considerations could be drawn from the spectral analysis of these motions. The power spectral densities
474 have been calculated for the whole set of 1281 records and the mean and top-third averaged surge and
475 sway spectra are shown in Fig. 15-16, respectively.

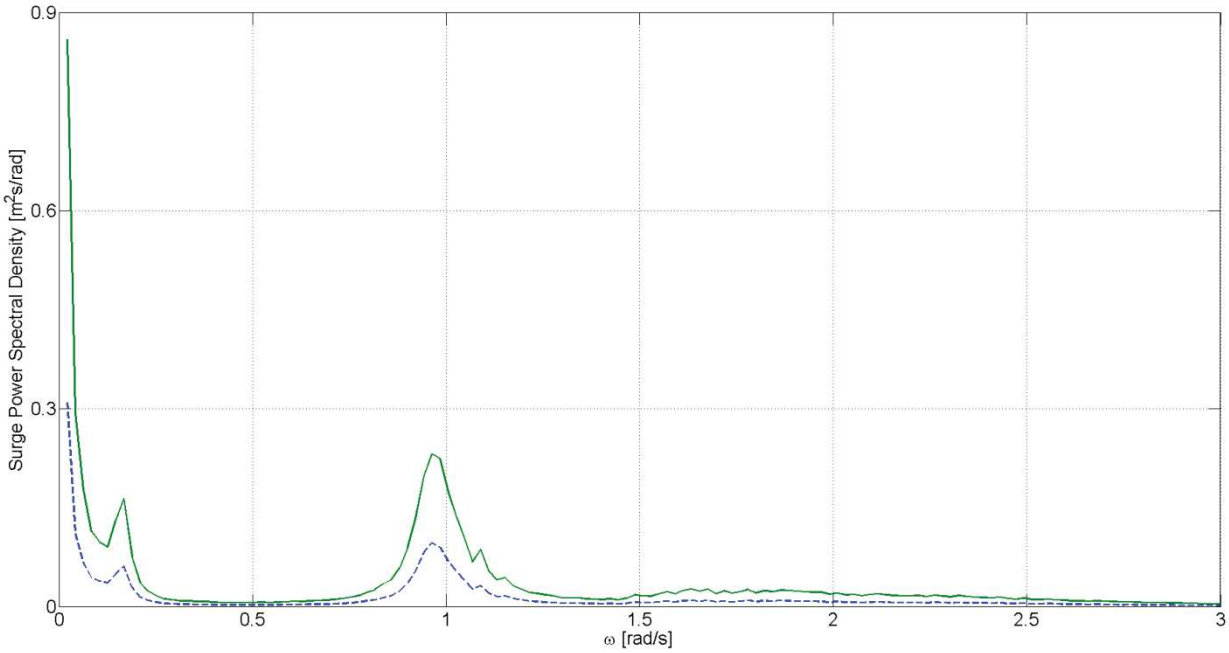

Figure 15 – Mean and top-third averaged surge response spectra of the whole dataset of 1281 sea states recorded during the experiment.

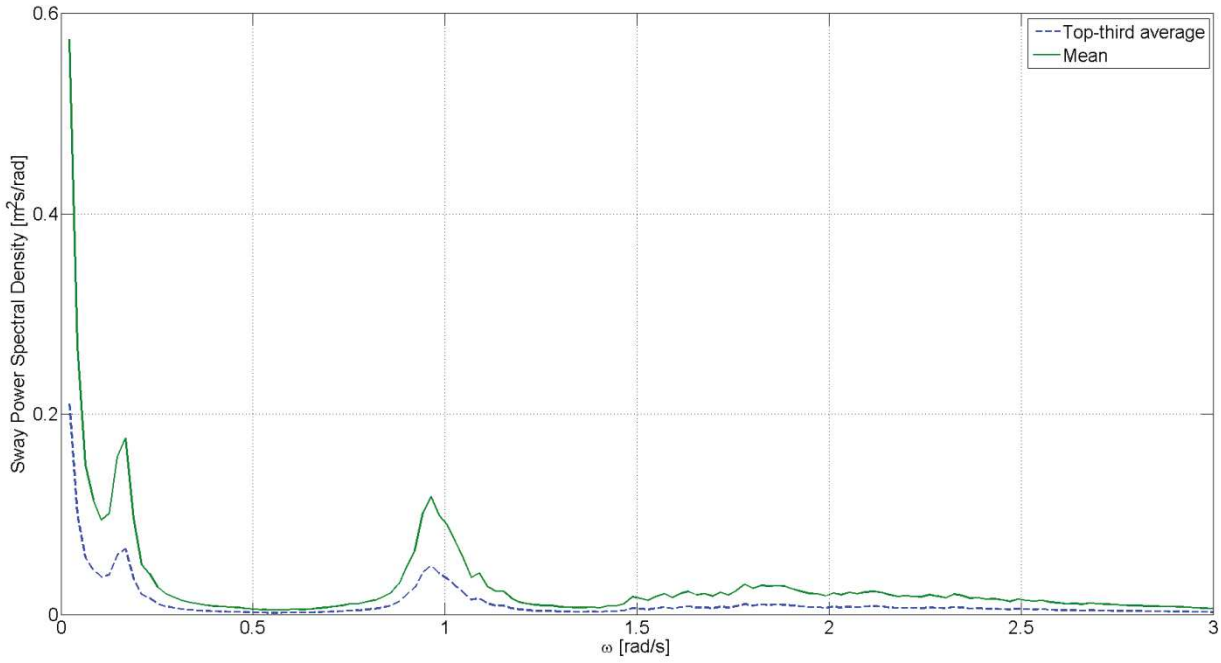

Figure 16– Mean and top-third averaged sway response spectra of the whole dataset of 1281 sea states recorded during the experiment.

The averaged power spectral densities shown in Fig. 15.16 may be divided in various regions, corresponding to different contributions. The first region (ω < 0.1 rad/s) is that of slow-drift motions, which may be induced by wind, currents and/or tidal, as well as by slow-drift wave forces. The second region corresponds to surge and sway natural frequencies, which are equal to each other: $\omega_1 = \omega_2 = 0.168$ rad/s. This result confirms that the stiffness values in surge and sway are close to each other, in spite of the geometric asymmetry of the mooring system. It should be also noted that the range of natural frequencies of the

individual power spectral densities span from ω = 0.147 rad/s to ω = 0.189 rad/s. This is due to the nonlinear mooring stiffness and to the randomness of wave energy content distribution (thought small) in the corresponding frequency range. The third region shows the coupling between surge/sway and pitch/roll, as well as a small coupling with heave motion. The frequencies of the corresponding peaks in Fig. 15-16 are respectively ω = 0.963 rad/s to ω = 1.089 rad/s, which are consistent with the values reported in Tables 5-6. Also in this case, the individual power spectral densities show a variability of the natural frequencies, which is due to nonlinear effects and should be further addressed in further time-domain analyses of the experimental results. Finally, the fourth region (ω > 1.1 rad/s) corresponds to the wave-induced motions, which are smaller than the other contributions in average but are significant for individual wind-generated sea states. Although the analysis of response spectra gives some clear information about the dynamic behaviour of the model in surge and sway degrees of freedom, it could not be used for direct estimation of the corresponding linear damping coefficients necessary for the calibration of the numerical model. To this aim, the Authors proposed an alternative identification method [43], based on the adoption of output-only identification techniques, borrowed from Operational Modal Analysis. This approach has already proved successful for the dynamic identification of a numerical model of a spar structure, similar to the present one, and may be hence used in future studies to complement the identification process of the intermediate-scale models of offshore structures installed at sea.

Conclusions

This paper presents the results of an experimental activity on a 1:30 scale model of a spar floating support structure (OC3-Hywind) for offshore wind turbines, in parked rotor conditions. The experiment was conducted at sea, in the Natural Ocean Engineering Laboratory of Reggio Calabria (Italy), between July 2015 and March 2016. The aim of the experiment was to investigate the feasibility of intermediate-scale, open-sea experimental activities on floating support structures for offshore wind turbines, which may overcome some of the most relevant limitations of the traditional small-scale ones, namely the high costs, the introduction of significant scale effects, and the limited duration of the experimental campaigns. Traditional identification techniques, commonly adopted in wave tanks and ocean basins, could not be directly applied to the interpretation of the experimental data, due to the non-controlled nature of the marine environment, hence they have been opportunely modified to meet the requirements of the application considered. 1281 5-minutes long sea states, including wind-generated waves, mixed sea states, and swells have been measured, and they have been used to perform the dynamic identification of the model considered, and to calibrate its numerical model, implemented in ANSYS AQWA. The main conclusions are:

- An optimised approach for intermediate-scale, open-sea experiments of floating offshore wind turbines has been proposed. In particular, the requirements of a suitable test site have been identified, and some identification techniques compatible with the non-controlled marine environment have been proposed.
- The free decay tests provided a good estimation of the natural frequencies of the model, but proved to overestimate the linear damping coefficients.
- The irregular wave tests were used to estimate the natural frequencies, damping coefficients and Response Amplitude Operators (RAOs) in the operational wave conditions of the model. The experimental RAOs obtained match well with the numerical predictions, and allowed to calibrate the numerical model.

- The limited frequency range of the natural sea states recorded at the test site resulted in the impossibility of identify the dynamics of the model over the complete frequency range. This is an intrinsic limitation of the open-sea experiment, when traditional input-output identification techniques, such as those presented in this paper, are applied. Due to this limitation, experimental RAOs estimation and numerical model calibration could be performed only for heave, roll and pitch degrees of freedom of the model.
- Some alternative approaches have been proposed to overcome the above limitations. Spectral analysis of surge and sway motions has proved to be suitable for identifying the corresponding natural frequencies and the most relevant dynamic characteristics. Finally, output-only identification techniques typical of Operational Modal Analysis [43] have been suggested as potential alternative/complementary methods for the full identification of intermediate-scale models of floating structures installed at sea.

Acknowledgements and competing interests

The activity has not been supported by any specific project.

The Authors have no competing interests to declare.

References

[1] Mast E, Rawlinson R, Sixtensson C. Market study floating wind in the Netherlands. DNV GL, TKI Wind op Zee. Available at: http://www.tki-windopzee.nl/files/2016-02/20160111-rap-market.study.floating.wind-lba-v02.pdf. Accessed July 2017.

[2] Failla G, Arena F. New perspectives in offshore wind energy. Philosophical Transactions of the Royal Society A: Mathematical, Physical and Engineering Sciences 2015; 373(2035). doi: 10.1098/rsta.2014.0228.

[3] Collu M, Borg M. Design of floating wind turbines. In Ng C, Ran L, editors. Offshore wind farms. Elsevier, 2016.

[4] Jonkman J, Musial W. Offshore Code Comparison Collaboration (OC3) for IEA Task 23 Offshore Wind Technology and Deployment. Technical Report NREL/TP-5000-48191. National Renewable Energy Laboratory (NREL), 2010.

[5] Robertson A, Jonkman J, Musial W, Vorphal F, Popko W, Qvist J, Froyd L, Chen X, Azcona J, Uzunoglu E, Guedes Soares C, Luan C, Yutong H, Pengcheng F, Yde A, Larsen T, Nichols J, Buils R, Lei L, Nygaard TA, Manolas D, Heege A, Vatne SR, Ormberg H, Duarte T, Godreau C, Hansen HF, Nielsen AQ, Riber H, Le Cunff C, Beyer F, Yamaguchi A, Jung KJ, Shin H, Shi W, Park H, Alves M, Guérinel M. Offshore Code Comparison Collaboration, Continuation within IEA Wind Task 30: Phase II Results regarding a Floating Semisubmersible Wind System. In: Proc. of the 33rd Int. Conf. on Offshore Mech. and Arctic Eng. (OMAE2014), ASME, June 8-13, San Francisco, California, USA, paper OMAE2014-24040; 2014..

[6] Martin HR, Kimball RW, Viselli AM, Goupee AJ. Methodology for Wind/Wave Basin Testing of Floating Offshore Wind Turbines. In: Proc. of the 31st Int. Conf. on Offshore Mech. and Arctic Eng. (OMAE2012), ASME; July 1-6, Rio de Janeiro, Brazil, paper OMAE2012-83627; 2012. .

[7] Goupee AJ, Guyedon SMH, Robertson AN. Floating wind turbine tank testing. In: Cruz J, Atcheson M, editors. Floating offshore wind energy. The next generation of wind energy. Cham: Springer; 2016.

[8] ITTC. Recommended procedure 7.5-02-07-03.8. 2014

[9] Ishida S, Kokubun K, Nimura T, Utsunomiya T, Sato I, Yoshida S. At-sea experiment of a hybrid spar type offshore wind turbine. In: Proc. of the 32nd Int. Conf. on Offshore Mech. and Arctic Eng. (OMAE2013), ASME, June 9-14, 2013, Nantes, France, OMAE2013-10655; 2013.

[10] Utsunomiya T, Matsukuma H, Minoura S, Ko K, Hamamura H, Kobayashi O, Sato I, Nomoto Y, Yasui K. On sea experiment of a hybrid SPAR for floating offshore wind turbine using 1/10 scale model. In: Proc. of the 29th Int. Conf. on Offshore Mech. and Arctic Eng. (OMAE2010), ASME, June 6-11, Shanghai, China, paper OMAE2010-20730; 2010.

[11] Viselli AM, Goupee AJ, Dagher HJ. Model test of a 1:8 scale floating wind turbine offshore in the Gulf of Maine. In: Proc. of the 33rd Int. Conf. on Offshore Mech. and Arctic Eng. (OMAE2014), ASME, June 8-13, San Francisco, California, USA, OMAE2014-23639; 2014.

[12] Statoil website. https://www.statoil.com. Accessed June 2017.

[13] Nielsen FG, Hanson TD, Skaare B. Integrated dynamic analysis of offshore floating wind turbines. Hamburg, Germany: Hydro Oil & Energy; 2006.

[14] Jonkman J. Definition of the floating system for phase IV of OC3. Technical Report NREL/TP-500-47535. National Renewable Energy Laboratory (NREL); 2010.

[15] Jonkman J, Butterfield S, Musial W, Scott G. Definition of a 5-MW reference wind turbine for offshore system development. Technical Report NREL/TP-500-38060. National Renewable Energy Laboratory (NREL); 2009.

[16] Shin H. Model test of the OC3-hywind floating offshore wind turbine. In: Proc. of the 21st Int. Offshore and Polar Eng. Conf. (ISOPE2011), June 19-24, Maui, HI, USA. p. 361-367; 2011.

[17] Chujo T, Minami Y, Nimura T, Ishida S. Experimental study for spar type floating offshore wind turbine with blade-pitch control. In: Proc. of the 32nd Int. Conf. on Offshore Mech. and Arctic Eng. (OMAE2013), ASME, June 9-14, Nantes, France, paper OMAE2013-10649; 2013.

[18] Utsunomiya T, Sato I, Yoshida S, Ookubo H, Ishida S. Dynamic response of a floating offshore wind turbine during severe typhoon event. In: Proc. of the 32nd Int. Conf. on Offshore Mech. and Arctic Eng. (OMAE2013), ASME, June 9-14, Nantes, France, paper OMAE2013-10618; 2013.

[19] Koo B, Goupee AJ, Lambrakos K, Kimball RW. Model tests for a floating wind turbine on three different floaters. In: Proc. of the 31st Int. Conf. on Offshore Mech. and Arctic Eng. (OMAE2012), ASME, July 1-6, Rio de Janeiro, Brazil, paper OMAE2012-83642; 2012.

[20] Goupee AJ, Koo B, Kimball RW, Lambrakos KF, Dagher HJ. Experimental comparison of three floating wind turbine concepts. In: Proc. of the 31st Int. Conf. on Offshore Mech. and Arctic Eng. (OMAE2012), ASME, Rio de Janeiro, Brazil, paper OMAE2012-83645; 2012.

[21] Sethuraman L, Venugopal V. Hydrodynamic response of a stepped-spar floating wind turbine: numerical modelling and tank testing. Renewable Energy 2013; 52: 160-174.

[22] Duan F, Hu Z, Niedzwecki JM. Model test investigation of a spar floating wind turbine. Marine Structures 2016; 49: 76-96

[23] Ruzzo C, Fiamma V, Nava V, Collu M, Failla G, Arena F. Progress on the experimental set-up for the testing of a floating offshore wind turbine scaled model in a field site. Wind Engineering 2016, 40(5): 455-467.

[24] Ruzzo C, Fiamma V, Failla G, Arena F, Collu M, Nava V. Open-sea 1:30 scale tests on a spar-type offshore wind turbine in parked conditions: Progress and future work. Progress in Renewable Energies Offshore – Proc. of the 2nd Int. Conf. on Renewable Energies Offshore (RENEW 2016), Lisbon, Portugal, pp. 609-616; 2016.

[25] ANSYS® , Academic Research, Release 16.1.

[26] ANSYS® AQWA, v. 16.1, Help System, Theory Manual, ANSYS, Inc.

[27] Boccotti P. Wave mechanics and wave loads on marine structures. 1st ed. Waltham: Elsevier; 2014.

[28] Arena F, Barbaro G. The Natural Ocean Engineering Laboratory, NOEL, in Reggio Calabria, Italy: a commentary and announcement. Journal of Coastal Research 2013; 29 (5): vii-x.

[29] Natural Ocean Engineering Laboratory (NOEL) website. Available at: http://noel.unirc.it/. Accessed July 2017.

[30] Bayati I, Belloli M, Bernini L, Mikkelsen R, Zasso A. On the aero-elastic design of the DTU 10 MW wind turbine blade for the LIFES50+ wind tunnel scale model. Journal of Physics: Conference Series 2016; 753(2): 022028.

[31] Bayati I, Belloli M, Bernini L, Fiore E, Gilberti H, Zasso A. On the functional design of the DTU 10 MW wind turbine scale model. Journal of Physics: Conference Series 2016; 753(5): 052018.

[32] Bayati I, Belloli M, Bernini L, Zasso A. Wind tunnel validation of AeroDyn within LIFES50+ project: imposed surge and pitch tests. Journal of Physics: Conference Series 2016; 753(9): 092001.

[33] Morison JR, O'Brien MP, Johnson JW, Schaaf SA. The force exerted by surface waves on piles. Petroleum transactions 1950; 189: 149-156.

[34] Det Norske Veritas. Environmental conditions and environmental loads. Recommended practice DNV-RP-C205. 2010.

[35] Sarpkaya T, Isaacson M. Mechanics of wave forces on offshore structures. Van Nostrand Reinhold Co. 1981; 1-650.

[36] Boccotti P, Arena F, Fiamma V, Barbaro G. Field experiment on random wave forces acting on vertical cylinders. Probabilistic Engineering Mechanics 2012; 28: 39-51.

[37] Boccotti P, Arena F, Fiamma V, Romolo A. Two small-scale field experiments on the effectiveness of Morison's equation. Ocean Engineering 2013; 57: 141-149.

[38] Robertson E, Jonkman J. Loads analysis of several offshore floating wind turbine concepts. In: Proc. of the 21st Int. Offshore and Polar Eng. Conf. (ISOPE2011), June 19-24, Maui, HI, USA. p. 443-450; 2011.

[39] Quallen S, Xing T, Carrica P, Li Y, Xu J. CFD simulation of a floating offshore wind turbine system using a quasi-static crowfoot mooring-line model. Journal of Ocean and Wind Energy 2014; 1(3): 143-152.

[40] Arena F, Guedes Soares C, Petrova P. Theoretical analysis of average wave steepness related to peak period or to mean period. In: Proc. of the 29th Int. Conf. on Offshore Mech. and Arctic Eng. (OMAE2010), ASME, June 6-11, Shanghai, China, paper OMAE2010-20811; 2010.

[41] Hasselmann K, Barnett TP, Bouws E, Carlson H, Cartwright DE, Enke K, Ewing JA, Gienapp H, Hasselmann DE, Kruseman P, Meerburg A, Muller P, Olbers DJ, Richter K, Sell W, Walden H. Measurements of wind wave growth and swell decay dur-ing the Joint North Sea Wave Project (JONSWAP). Deut. Hydrog, Zeit. 1973, A8: 1-95.

[42] Ribeiro e Silva S, Guedes Soares C, Prediction of parametric rolling in waves with a time domain non-linear strip theory model. Ocean Engineering 2013; 72: 453-469.

[43] Ruzzo C, Failla G, Collu M, Nava V, Fiamma V, Arena F. Operational modal analysis of a spar-type floating platform using frequency domain decomposition method. Energies 2016, 9(11), paper no. 870

A. Appendix

Parameter α of equation (14) has been calibrated through a parametric analysis on the whole dataset collected during the experiment. Ideally speaking, the domain of meaningful values for this parameter ranges from 0 to 1. In the limit case of α = 0, the response spectra of each sea state would be used for the determination of the RAOs in the whole frequency domain, including the portions where the wave spectrum ordinates are very small and their estimation is not accurate, due to the unavoidable numerical inaccuracies. Such a case would result in RAOs tending to infinite in these portions, and generally in strong inaccuracies in their estimation. In the opposite limit case of α=1, only the peak spectral ordinates would be used for the determination of the RAOs, resulting in a single point in the frequency domain for each sea state. While in this case the numerical inaccuracies in the spectrum determination would be negligible, the resulting estimation of the RAOs would be limited to few points in the frequency domain. In this study, the value of α has been set equal to 0.10 after a parametric analysis, aimed to evaluate its effect on the estimation of experimental RAOs. Similarly, frequency range has been limited to ω = (0.8 – 4.0) rad/s (1:30 scale), due to the scarcity of data out of this range.

The parametric analysis has been conducted by estimating the experimental RAOs for six different values of the parameter α of equation (14), ranging from 0.10 to 0.60. At this stage, the six estimates of the RAOs for each of the three degrees of freedom have been plotted on the frequency range ω = (0.0 – 5.0) rad/s. The results obtained are shown in Fig A1-A3.

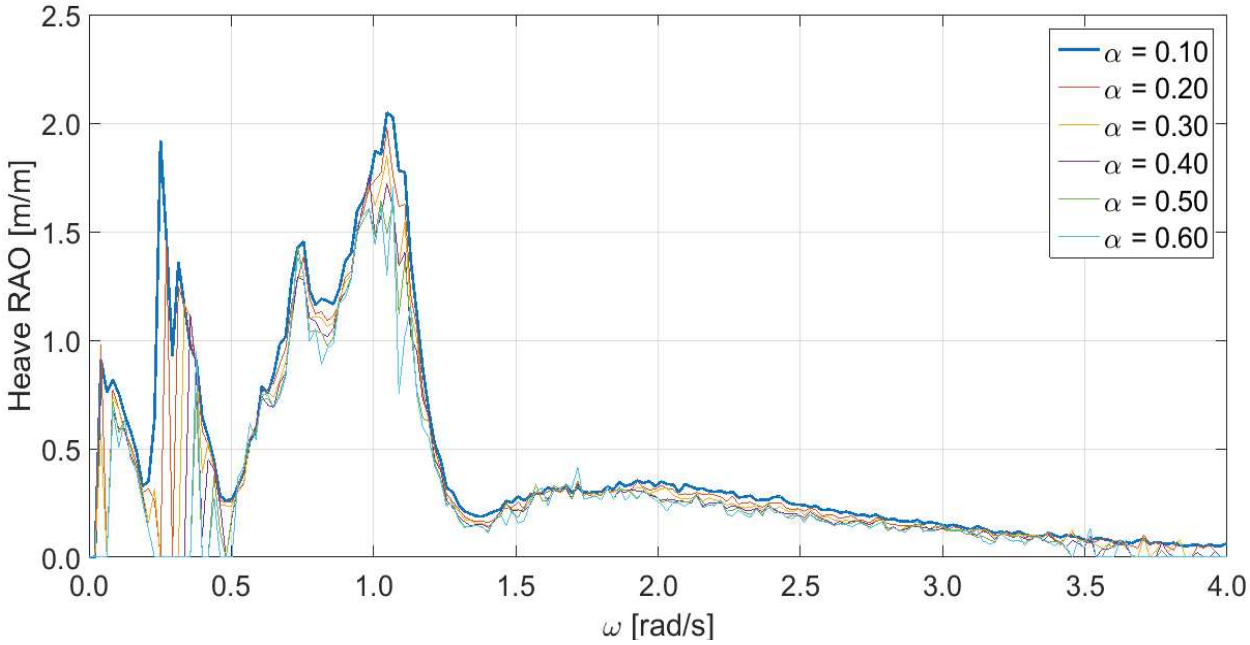

672

673 *Figure A1 – Experimental heave RAOs obtained for different values of α (1:30 scale).*

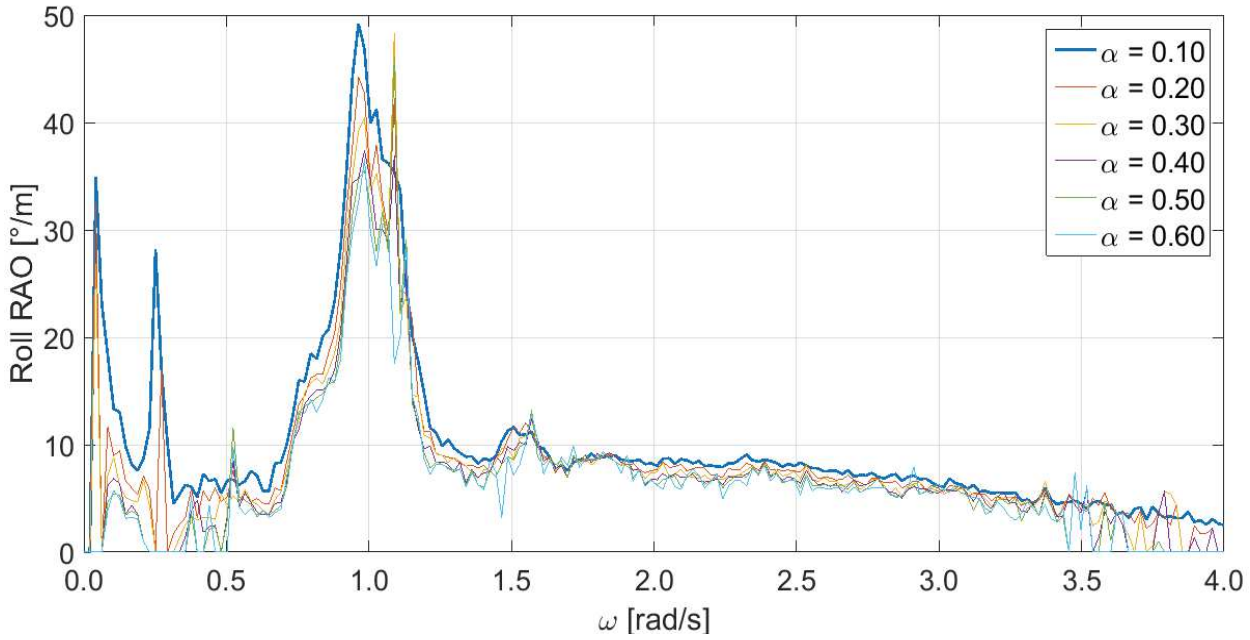

674

675 *Figure A2 – Experimental roll RAOs obtained for different values of α (1:30 scale).*

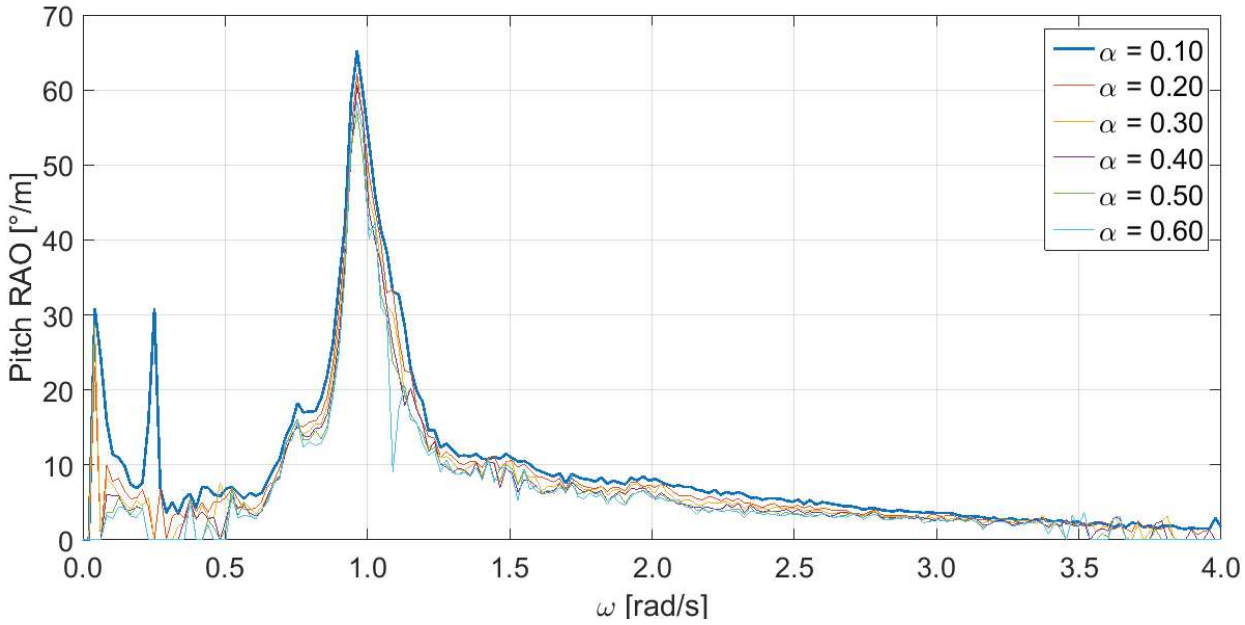

Figure A3 – Experimental pitch RAOs obtained for different values of α (1:30 scale).

Concerning the frequency range, as expected, the number of contributions (eq. 14) available for the averaging procedure is too small for the smallest and highest frequencies, resulting in inaccurate estimations in the corresponding portions of the frequency domain. Basing on the analysis of the wave data available (Fig. 8), the frequency range ω = (0.80 – 4.10) rad/s has been chosen for the estimation of the RAOs. It corresponds to a maximum wave period of about 8 s, which is consistent with the wave conditions observed at NOEL site (Fig 8). In the selected frequency range, the global shape of the RAOs is not significantly altered by the variation of α. This confirms the robustness of the calculation procedure, provided that sufficient wave data are available. However, the RAOs corresponding to α = 0.10 are significantly smoother than the other ones. This is due to the fact that larger values of α involve a significant decrease of the number of contributions (eq. 14) to the average estimate at certain frequencies. This phenomenon is particularly evident for the roll RAO at the frequency ω = 1.089 rad/s. As a consequence, for the case study considered, the value α = 0.10 has been chosen. Higher values for α can be used by increasing the number of samples in the dataset used in the calibration.